Sumecton reinforced gelatin-based scaffolds for cell-free bone regeneration

Lukin, Izeia; Erezuma, Itsasne; Garcia-Garcia, Patricia; Reyes, Ricardo; Evora, Carmen; Kadumundi, Firoz Babu; Dolatshahi-Pirouz, Alireza; Orive, Gorka

Published in:
International Journal of Biological Macromolecules

Link to article, DOI:
10.1016/j.ijbiomac.2023.126023

Publication date:
2023

Document Version
Publisher's PDF, also known as Version of record

International Journal of Biological Macromolecules 249 (2023) 126023

Contents lists available at ScienceDirect

International Journal of Biological Macromolecules

journal homepage: www.elsevier.com/locate/ijbiomac

Sumecton reinforced gelatin-based scaffolds for cell-free bone regeneration

Izeia Lukin [a,b], Itsasne Erezuma [a,b], Patricia Garcia-Garcia [c], Ricardo Reyes [d], Carmen Evora [c], Firoz Babu Kadumudi [e], Alireza Dolatshahi-Pirouz [e], Gorka Orive [a,b,f,g,h,*]

[a] NanoBioCel Research Group, School of Pharmacy, University of the Basque Country (UPV/EHU), Vitoria-Gasteiz, Spain
[b] Bioaraba, NanoBioCel Research Group, Vitoria-Gasteiz, Spain
[c] Department of Chemical Engineering and Pharmaceutical Technology, Universidad de La Laguna, 38200 La Laguna, Spain
[d] Department of Biochemistry, Microbiology, Cell Biology and Genetics, Universidad de La Laguna, 38200 La Laguna, Spain
[e] Department of Health Technology, Technical University of Denmark (DTU), 2800 Kgs. Lyngby, Denmark
[f] Biomedical Research Networking Centre in Bioengineering, Biomaterials and Nanomedicine (CIBER-BBN), Vitoria-Gasteiz, Spain
[g] BTI-Biotechnology Institute, Vitoria, Spain
[h] University Institute for Regenerative Medicine and Oral Implantology - UIRMI (UPV/EHU-Fundación Eduardo Anitua), Vitoria-Gasteiz, Spain

ARTICLE INFO

Keywords:
3D scaffold
Bone
Biomaterials
Gelatin
Nanoclays
SDF-1

ABSTRACT

Bone tissue engineering has risen to tackle the challenges of the current clinical need concerning bone fractures that is already considered a healthcare system problem. Scaffold systems for the repair of this tissue have yielded different combinations including biomaterials with nanotechnology or biological agents. Herein, three-dimensional porous hydrogels were engineered based on gelatin as a natural biomaterial and reinforced with synthetic saponite nanoclays. Scaffolds were biocompatible and shown to enhance the inherent properties of pristine ones, in particular, proved to withstand pressures similar to load-bearing tissues. Studies with murine mesenchymal stem cells found that scaffolds had the potential to proliferate and promote cell differentiation. *In vivo* experiments were conducted to gain insight about the ability of these cell-free scaffolds to regenerate bone, as well as to determine the role that these nanoparticles in the scaffold could play as a drug delivery system. SDF-1 loaded scaffolds showed the highest percentage of bone formation, which was corroborated by osteogenic markers and new blood vessels. Albeit a first attempt in the field of synthetic nanosilicates, these results suggest that the designed constructs may serve as delivery platforms for biomimetic agents to mend bony defects, circumventing high doses of therapeutics and cell-loading systems.

1. Introduction

Bone fractures are already considered a problem for the global health system. A recent study has shown that since 1990 there has been an increase in new bone fractures as well as in long-term symptoms, 33,4 % and 70 %, respectively and it is expected to reach 23 % in 2030 [1,2].

In this sense, tissue engineering aims to address this worldwide concern by combining materials, engineering and biology science [3,4]. Specifically, bone tissue engineering (BTE) is focused on designing scaffolding systems (scaffolds, hydrogels, nanoparticles) to repair bone damaged area [5–7]. In the attempt to design a system to resemble this tissue in the best possible embodiment, merging new approaches- such as, nano and microengineering, bioprinting or freeze-drying- with the biomaterials used so far, has helped to generate systems ranging from drug or cell release systems to smart systems [8,9]. The latter are stimuli-responsive constructs that respond to changes in pH or temperature, for instance, and make them better mimic native tissue and possible variations that may happen in the tissue over time [10,11].

Among other biomaterials, gelatin has been extensively employed in tissue engineering area [12–17]. This collagen-derived natural polymer is mainly obtained from mammals, which allows to be properly integrated into the living organism. This confers properties such as good biocompatibility, biodegradability and low toxicity. In addition, RGD sequences in its chains can help cell adhesion, proliferation and differentiation [18]. Moreover, it is easy to handle and economical, making it an ideal composite for tissue engineering.

When it comes to BTE, this biomaterial is widely used because its precursor, collagen, is the main component of the organic part of this tissue [19]. However, as gelatin is thermosensitive, its chains usually have to be crosslinked to constitute gel form [12,13]. The latter is a key

* Corresponding author at: NanoBioCel Research Group, School of Pharmacy, University of the Basque Country (UPV/EHU), Vitoria-Gasteiz, Spain.
E-mail address: gorka.orive@ehu.eus (G. Orive).

https://doi.org/10.1016/j.ijbiomac.2023.126023
Received 18 May 2023; Received in revised form 19 July 2023; Accepted 25 July 2023
Available online 26 July 2023

Table 1
Gelatin-Sumecton reinforced scaffolds composition.

	Gelatin % (w/v)	Microbial transglutaminase	Sumecton % (w/v)
SUM0	10	100 mg/mL	0
SUM0.5			0.5
SUM1			1
SUM2			2

step that occasionally can be challenging, and it may prevent gelatin from being a part of injectable system. Nonetheless, studies have demonstrated that adding functional groups to this polymer, such as, methacrylated groups can reduce crosslinking time as well as increase injectability [20,21].

Unfortunately, most of gelatin-based systems lack of consistency to support bone regeneration. To overcome that issue, different alternatives have been explored. Adding inorganic particles- such as hydroxyapatite or calcium- to hydrogels have resulted in better mimicking bone tissue [12,22]. Latest trends are shifting towards nanoparticles, nanoclays among others.

Nanoclays turn out to be nanosized silicates with Ag, Mg within their two-dimensional structure. These complex constructions are capable of both reinforcing already designed scaffolds and repairing bone regeneration by means of the array minerals these nanomaterials contain in their network [23–25]. Extensive studies described the osteoregenerating capacity of laponite and montmorillonite nanoclays [23,26]. Still, there are others that are less frequently reported. A recent study has examined an array of nanoclays for bone regeneration purposes and among them was synthetic saponite [27].

In the direction of gathering more information and acquiring knowledge about this synthetic nanosilicate, the present work introduces novel nanoreinforced scaffolds with gelatin for bone tissue engineering purposes. To accomplish the latter, saponite derived synthetic nanoclay (Sumecton) has been incorporated to enzymatically crosslinked gelatin network. Scaffolds were characterized in terms of swelling, degradation and protein adsorption capability. Culturing murine bone-marrow derived mesenchymal stem cells (mBM-MSCs) on top of fabricated hydrogels determined biological potential of matrices. Ultimately, *in vivo* studies displayed the capacity for hydrogels to regenerate bone defects.

2. Materials and methods

2.1. Materials

Bovine skin derived gelatin (Type B, ~225 g Bloom), Cell Counting Kit-8 (CCK-8), collagenase P from *Clostridium hystoliticum*, bovine serum albumin (BSA), *p*-nitrophenyl phosphate (pNPP), calf intestinal alkaline phosphatase (CIAP), dexamethasone, ascorbic acid and β-glycerophosphate were acquired from Sigma Aldrich, Spain. Ajinomoto Foods Europe (France) provided microbial Transglutaminase (100 U/g) and Sumecton SA nanoclay from Kunimine Industries CO., Ltd., Japan. Mouse fibroblast L-929 cell line, culture media Dulbecco's Modified Eagle's Medium (DMEM 30-2002) and Eagle's Minimum Essential Medium (EMEM 30-2003) were purchased at ATCC (Spain). Phosphate Buffered saline (PBS), Trypsin, fetal bovine serum (FBS), Penicillin-Streptomycin solution, Pierce™ BCA Protein Assay Kit, LIVE/DEAD® kit and 5-bromo-4-chloro-3-indolyl phosphate/nitroblue tetrazolium (BCIP/NBT) were acquired from Fisher Scientific (Spain). TRIsureTM and SensiFAST Probe Hi-ROX Mix reagents were purchased from Bioline, recombinant mouse SDF1 alpha protein (SDF-1) from Abcam and human bone morphogenetic protein-2 (BMP-2) from GenScript.

2.2. Preparation of nanoreinforced gelatin-Sumecton scaffolds

Gelatin-based three-dimensional (3D) scaffolds were fabricated as previously described by Echave et al. [13]. In brief, 10 % w/v gelatin solution was prepared and for that, gelatin (1 g) was dissolved in distilled water at 40 °C over 1 h in continuous agitation. Concurrently, enzyme solution (100 mg/mL) was prepared with 20 U/g gelatin activity microbial transglutaminase and distilled water. To reinforce the solution, varying quantities of Sumecton were added (Table 1).

Gelatin dispersions with or without Sumecton were blended with enzyme solution and briefly homogenized under magnetic stirring, subsequently transferred to 100 mm Petri dishes and kept at 4 °C for 1 h to completely crosslink them. Resulting hydrogels were composed of gelatin (10 % w/v) and 20 U/g gelatin enzyme was used to obtain completed crosslinked systems. Hydrogels were then punched to create 3D cylindrical scaffolds of the chosen size. The constructs were soaked in ethanol (70 % v/v) for 15 min, followed by several washes with PBS to rests of ethanol. Samples were subsequently frozen at −80 °C, then lyophilized.

2.3. Swelling behavior and degradation performance

Swelling phenomena of engineered scaffolds was ascertained in PBS at 37 °C under continuous stirring (300 rpm). An initial dried weight of each sample was determined before their immersion in PBS. At the end of each period of time (1, 2, 5, 10, 15 and 30 min, 1, 2, 7, and 24 h) the wet sample weight was acquired, after the excess of the surface liquid was removed. The swelling ratio was estimated according to Eq. (1): Ws is the wet sample weight and Wo refers to the initial dry weight on the same sample.

$$\text{Swelling Ratio} = (Ws - Wo)/Wo \quad (1)$$

Tests for hydrolytic and enzymatic degradation were carried out to simulate the behavior of the samples in physiological environment. At the hydrolytic degradation experiment, scaffolds were initially soaked in PBS up to the swelling equilibrium (2 h) and subsequently weighed. On this basis, the baseline was set as the initial weight and the samples were then placed in PBS and incubated at 37 °C for 21 days. After completion of the incubating period, samples were withdrawn and each sample's weight was registered. Degradation ratio was calculated by weighing the remnant samples. In the enzymatic degradation assay, samples were submerged in 0.02 % collagenase P mixture (w/v). Protein concentration was ascertain in every time point (5, 15, 30 min and 1, 4 h). After total degradation of the prototypes, the total amount of protein found in the supernatant was also quantified using commercially available kits, as instructed by the supplier.

2.4. Protein adsorption studies

In this study, lyophilized scaffolds were hydrated in PBS and weighed prior to assay. Hydrogels were soaked during 24 h in 37 °C in 1 mg/mL BSA mixture with steady stirring and washed several times to remove all unbound BSA. 2 % sodium dodecyl sulfate solution (SDS, Sigma-Aldrich) removed all protein. Then, BSA concentration of each scaffold was measured by MicroBCA™ assay (Thermo Scientific) following manufacturer's protocol. Results are expressed in μg of absorbed BSA for mg of hydrogel.

2.5. Physicochemical characterization

2.5.1. Chemical composition: Fourier Transform Infrared (FTIR) spectroscopy and X-ray powder diffraction (XRD) analysis

FTIR spectroscopy determined the chemical arrangement of freeze-dried hydrogels. All samples were recorded with the FTIR spectrometer (PerkinElmer Spectrum 100) in the 4000–500 cm^{-1} range with 16 scans at a resolution of 4 cm^{-1} and registered on attenuated total reflection. Collected spectra was adjusted to baseline and normalized with PerkinElmer Spectrum software.

XRD analysis of the freeze-dried samples was conducted with a X-ray

diffractometer (HUBER G670, Germany). Cu monochrome X-ray tube and a Cu secondary X-ray tube were provided in the diffractometer. Scan was completed in the range 2θ of 10–80° at 0.005° step size. The sealed tube X-ray generator was operated at the following conditions: 40 kV, 40 mA and Cu Kα1 radiation was provided at a 1.54056 Å wavelength.

2.5.2. Scanning electron microscopy (SEM)

SEM served to ascertain the porous structure of designed scaffolds. After lyophilizing hydrogels, they were cross-sectioned and gold sputtered (10 nm). Acquisition of images was performed at 5 kV accelerating voltage with Quanta FEG 250 (ESEM). Pore size and porosity were measured by ImageJ. Mineral formation within the scaffolds was also determined by SEM 5 weeks post-incubation. SEM analysis was performed under the same conditions as aforementioned.

2.5.3. Mechanical compressive properties

The mechanical performance of the engineered constructs was evaluated with Instron (model 5967, U.K.). Compression tests were performed using a load cell of 50 N at 0.5 mm/min compression speed. Prior to testing, the cylindrical scaffolds (8 mm diameter and 2 mm in depth) were immersed in PBS for 24 h and, before compression, the height and diameter of the designed scaffolds were measured with a Vernier caliper. The elastic modulus of scaffolds was estimated using the slope of the stress-strain curve in the 15–25 % strain region and ultimate stress was determined as maximum stress. The area under the stress-strain curve was used to calculate toughness.

2.6. Biocompatibility study

Mice-derived L-929 fibroblasts were cultured in EMEM 30-2003 medium complemented with 10 % FBS (v/v) and 1 % penicillin-streptomycin (v/v). Cell cultures were incubated at 37 °C with 5 % CO_2 and humidified-controlled environment and cell division was regularly performed when cells achieved confluence. Cell compatibility of the designed scaffolds was evaluated as described by Echave et al. [13], according to ISO 10993 guideline (Biological evaluation of medical devices guideline: cytotoxicity on extracts and cytotoxicity by direct contact). Cytotoxicity caused by direct interaction between cells and scaffold as well as non-direct toxicity were both evaluated by assessing the metabolic cell activity by means of colorometric assay (CCK-8 assay). 100 % viability was defined as the metabolic activity of cells that were not in contact with either the target scaffolds or the extracts.

2.7. Cell studies: murine bone-marrow derived mesenchymal stem cells (mBM-MSCs)

mBM-MSCs expansion was carried out in complete basal medium consisting of DMEM complemented with 10 % (v/v) FBS and 1 % (v/v) penicillin/streptomycin. Cell culture was executed in a controlled air (5 % CO_2) at 37 °C. The division of cells was conducted after they achieved confluence and all cellular studies were performed with cells at passage 8–10.

Prior to seeding the cells on the surface of the 3D platforms, every scaffold was subjected to ultraviolet light during 15 min and hydrated with culture medium overnight. Hydrated 3D constructs were set in wells and seeded 10^5 mBM-MSCs on the top of each scaffold. Thereafter, scaffolds were incubated in the CO_2- enriched incubator over 1.5 h followed by the addition of complete basal medium or bone-conditioned medium (supplemented with 0.5 μM dexamethasone, 200 μM ascorbic acid and 10 mM β-glycerophosphate) in every well. During tests, cell culture media was replaced at 2–3 days interval.

2.7.1. Cell viability study

Cell-viability was determined by MACSQuant Analyzer flow cytometer (Miltenyi Biotec) on days 1 and 8 post-seeding. After staining cells with Live/Dead kit, cells were fixed (4 % formaldehyde solution) for 30 min. Scaffolds were degraded with collagenase P solution 0,1 % (w/v). Centrifugations allowed the separation of the biomaterial from cells, which were then measured by the flow cytometer.

Quantitative data of cell viability was further complemented with microscopical images with Live/Dead viability kit following guidelines was tested in gelatin-based scaffolds. After 8 days of cell-seeding four samples per prototype were evaluated (SUM0, SUM0.5, SUM1). A solution of Calcein-AM and ethidium served to dye viable and non-viable cells, respectively. Microscope fluorescence images were acquired with the Nikon TMS inverted microscope.

2.7.2. Osteogenic studies

2.7.2.1. Alkaline phosphatase (ALP): activity and staining. ALP-secreted from cells was assessed weekly with a spectrophotometer for 21 days. Intracellular enzyme activity was determined at pH 9.3 by means of pNPP hydrolysis. A formulation based on CIAP together with 0.2 % (w/v) pNPP served as standard curve and mixed with the samples. As a final step, the reaction was stopped by a 3 M NaOH solution and absorbance at 405 nm was measured. At the final stage, cell-seeded were stained with BCIP/NBT mixture. After rinsing the constructs with PBS three times, samples were light-protected with the solution and incubated at RT over 2 h. The excessive amount of dye was then removed from scaffolds with PBS and observed under brightfield employing Nikon AZ100 microscope.

2.7.2.2. Gene expression approach. Reverse transcription-quantitative polymerase chain reaction (RT-qPCR) analysis. After obtaining RNA from mBM-MSCs by TRIsure reagent, High-Capacity cDNA Reverse Transcription Kit (Applied Biosystems) was employed to reversely transcribed 2 μg of total RNA and obtain complementary DNA (cDNA). SensiFAST Probe Hi-ROX Mix completed quantitative real-time PCR (StepOnePlus™ Real-Time PCR System). Genes were analyzed with Taqman 5′ - nuclease probe method (Applied Biosystems) and normalized with Glyceraldehyde-3-Phosphate Dehydrogenase (GADPH). Fold-change expression was estimated by the 2-ΔΔCt.

2.8. In vivo studies

Animal studies were conducted following the European Directive (2010/63/UE) on Care and Use of Animals in Experimental Procedures. Ethics Committee for Animal Care of the University of La Laguna (CEIBA2014-0128) approved in advance all mice procedures. Surgeries were executed under isoflurane anesthesia. Before incision, analgesia was administered: subcutaneous 0.05 mg/kg buprenorphine and 70 mg/kg paracetamol in drinking water, over 3 post-surgery days. After post-operative recovery, animals were allowed free movement, food and water.

Overall, *in vivo* studies were performed with SUM1 scaffolds. For this purpose, animals were divided into following groups: blank scaffolds, scaffolds loaded with BMP-2 (600 ng) or SDF-1 (1 ng) and scaffolds containing BMP-2 and SDF-1 (Fig. 9a).

2.8.1. Animal surgery

Animals underwent surgery with the purpose of causing calvaria bone tissue defect. Surgery was performed under general anesthesia with isoflurane and mice body temperature was controlled by a heated platform at 37 °C. Afterwards, scaffolds containing different treatments were embedded. Concisely, using a biopsy punch, a circular area of 4 mm was formed in the calvaria bone. A 4 mm circular transosseous defect was then composed with a trephine bur [28]. Scaffolds were placed into defects and skin was stapled on each animal. Eight weeks after the implantation animals were sacrificed *via* CO_2 inhalation and calvaria were extracted.

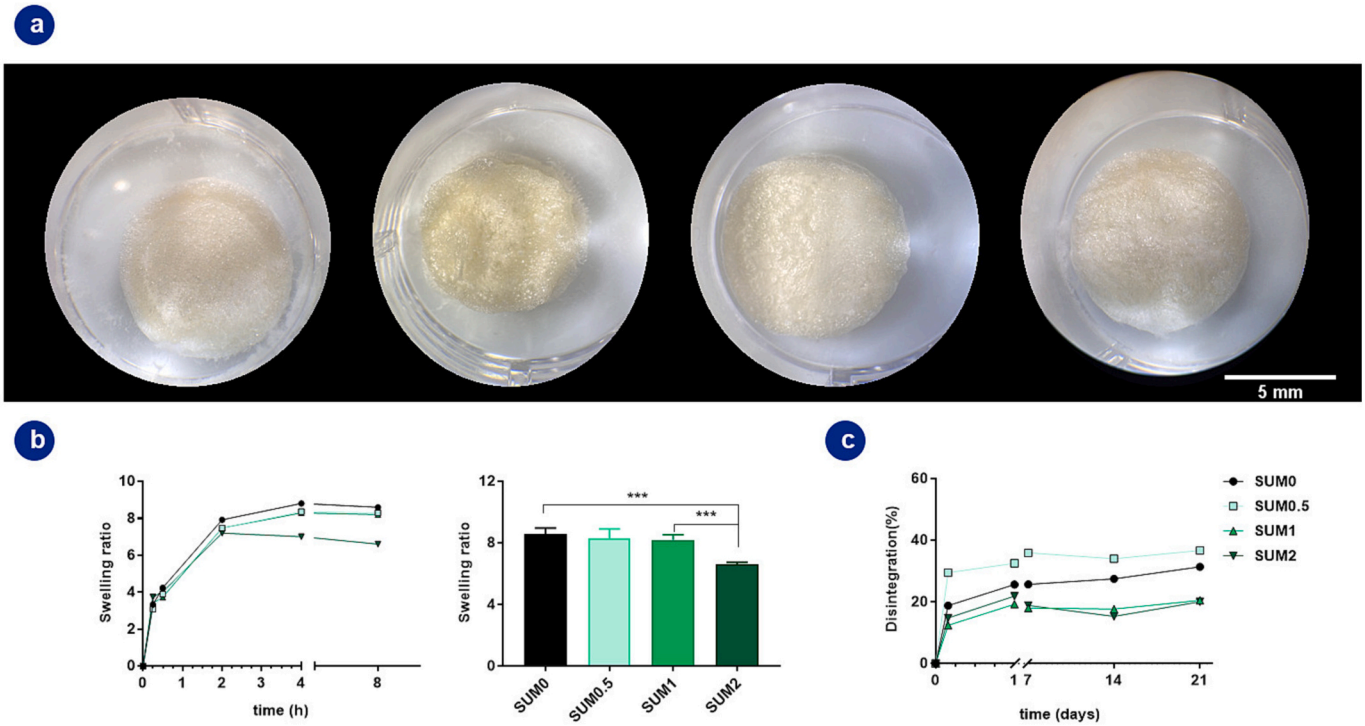

Fig. 1. Characterization of gelatin-Sumecton based scaffolds. (a) Macroscopical images of lyophilized 3D scaffolds. Scale bar = 5 mm. (b) Swelling profile and swelling ratio after 24 h of hydration. (c) Hydrolytic degradation profile.

2.8.2. Histology, histomorphometry and immunohistochemistry

To ascertain the potential of the scaffolds at regenerating the pre-created critical size defect, extracted samples were histologically analyzed as earlier explained [29]. In brief, samples underwent fixation with 4 % paraformaldehyde solution, decalcification using Histofix® Decalcifier (Panreac, Barcelona, Spain) and dehydratation by using graduated ethanol series Finally, samples were fixed in paraplast®. Each sample was sectioned longitudinally in 5 μm thick sections with a microtome (Shandon Finesse 325) and then dyed with hematoxylin-erythrosin to analyze newly formed bone. VOF trichrome dye assessed bone mineralization: red and brown tie denotes late-stage mineralization, while, less mineralized and new bone is dyed blue [30]. Sections were examined under light microscopy (LEICA DM 4000B) and analyzed then with computer based image analysis software Leica Q-win V3 Pro-image Analysis System (Barcelona, Spain). A region of interest (ROI) was defined within the lesion (12.5 mm^2) for quantitative assessment of new bone growth. Neoformation of the bone was calculated as a percentage of repair in comparison to the original defect area within the ROI.

As for immunohistochemical analysis, sections had to be deparaffined and rehydrated in Tris-buffered saline (TBS) (pH 7.4, 0.01 M Trizma base, 0.04 M Tris hydrochloride, 0.15 M NaCl), used for subsequent incubations and rinsing. Antigen retrieval was performed by incubating the sections in citrate buffer (pH 6) at 90 °C and hydrogen peroxide (0.3 %) for 20 min. Sections were blocked with 2 % FBS in TBS–0.2 % Triton X-100 (blocking buffer) after rinsing. For indirect assay sections were incubated with collagen type I (Col I) and osteocalcin (OCN) polyclonal antisera (1/100) (Millipore, Barcelona, Spain) in blocking buffer at 4 °C and overnight.

These sections underwent three washes and then incubation with biotin-SP-conjugated donkey anti-rabbit F(ab) fragment (1/500) (Millipore, Barcelona, Spain). Subsequently, sections were rinsed to incubate in peroxidase-conjugated streptavidin (1/500) (Millipore, Barcelona, Spain) through 1 h. Peroxidase activity was determined by Tris–HCl buffer (0.05 M, pH 7.6) comprising 0.005 % of 3.3′ diaminobencidine (Sigma, Poole, UK) and 0.01 % hydrogen peroxide. The specific antiserum was substituted with standard serum to determine the specificity of the reaction.

COL I and OCN staining were evaluated by ImageJ (NIH, Bethesda, MD) computer-based image analysis software. A set threshold within the ROI served to select positive staining and measure OCN and COL I staining. Pixel-positive regions were divided by the total surface size (mm^2) of the ROI and normalized with blank scaffolds. Values were reported as relative staining intensities.

The density of blood vessels together with the surface area of vessels within the ROI determined neovascularization. For that, an anti-CD34 monoclonal antibody (1/50) (DAKO, Barcelona, Spain) during the night at 4 °C in blocking solution marked the sections. Then, they were rinsed up to three times prior to 1 h incubation in blocking buffer with biotin-SP-conjugated donkey anti-rabbit F(ab) fragment (1/500). Subsequently, sections were rinsed to incubate in peroxidase-conjugated streptavidin (1/500) through 1 h. Peroxidase activity was ascertained by Tris–HCl buffer (0.05 M, pH 7.6) containing 3.3′ diaminobencidine (0.005 %) and hydrogen peroxide (0.01 %). Substituting the specific antiserum with normal one corroborated the reaction specificity. To express blood vessel density, absolute values were employed and vessel surface area (mm^2) was measured based on the quantitative assessment of ROI.

2.9. Statistical analysis

Analysis of statistical data was concluded with SPSS.25 software. Shapiro-Wilk test estimated normal distribution of the data. Data following a normal distribution were tested by one-way ANOVA to analyze the differences between the groups. For multiple comparisons, Tukey post-hoc test was employed. In all cases, p-values <0.05 were assumed to be significant, and displayed following the symbols of the graphs. All results are presented as mean ± standard deviation.

3. Results and discussion

Sumecton-reinforced 3D scaffolds were fabricated by enzymatic crosslinking and freeze-drying. While the organic section constituted an

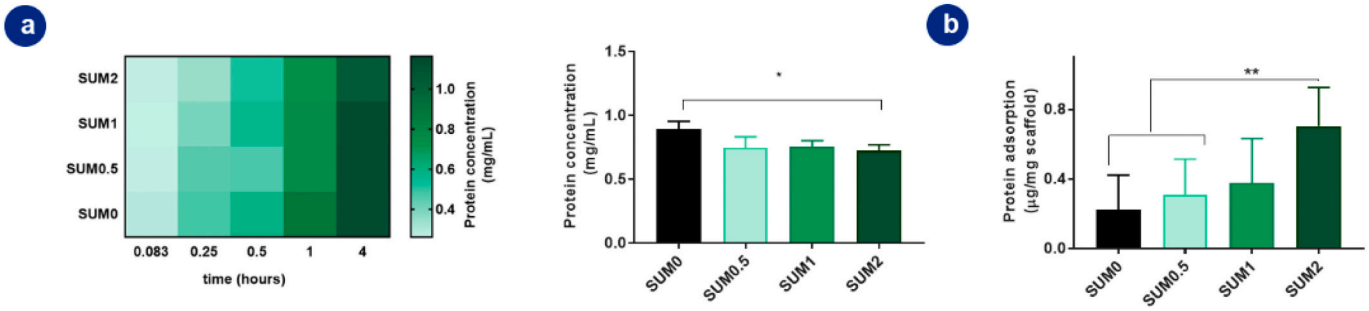

Fig. 2. Characterization of gelatin-Sumecton based scaffolds. (a) Combinatorial heat diagram of protein concentration after enzymatic degradation. (b) Protein adsorption study. Statistical significance: *p < 0.05, **p < 0.01, *** p < 0.001.

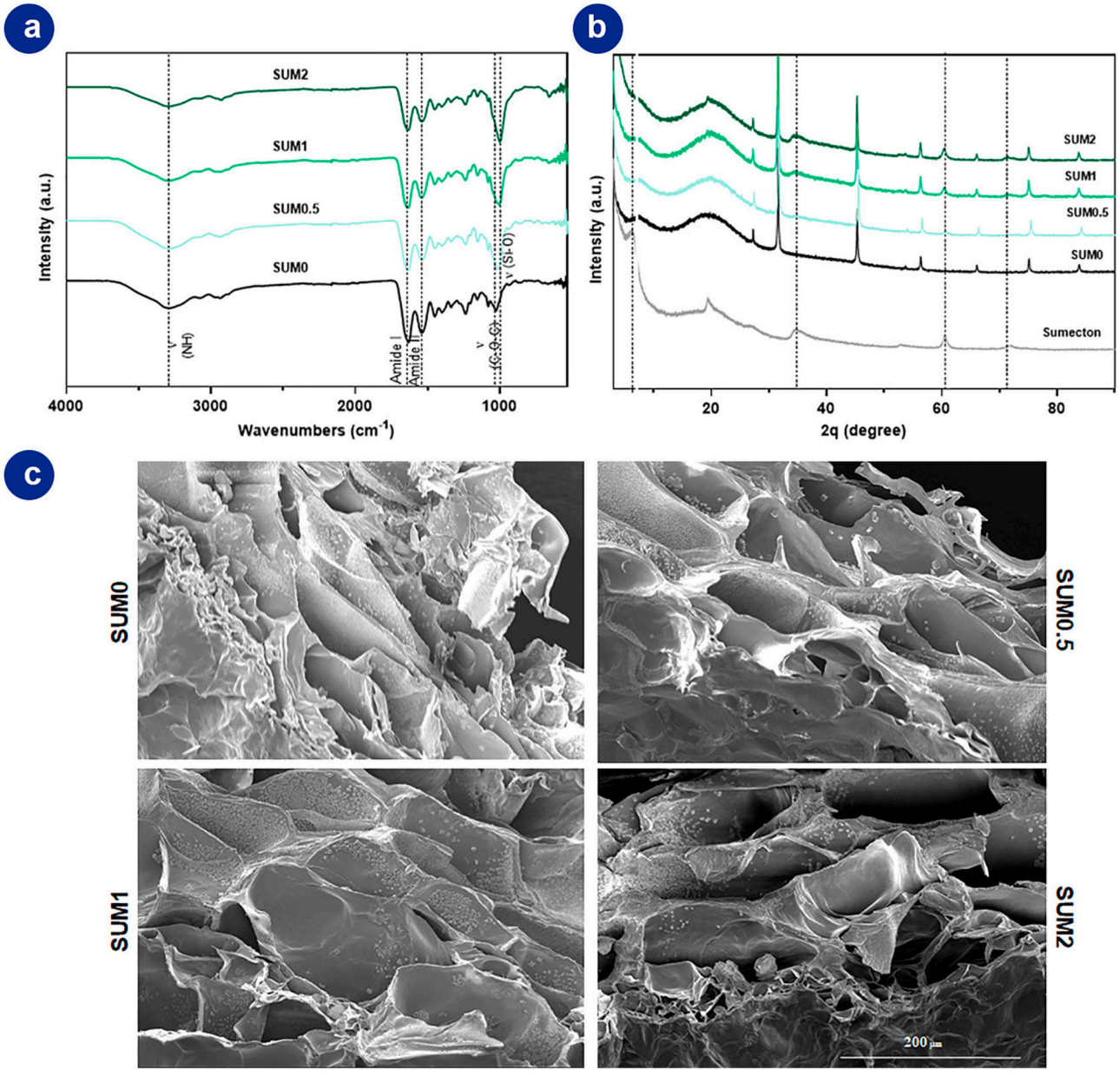

Fig. 3. Chemical and biomechanical studies. (a) Fourier transform infrared (FTIR) spectra of fabricated scaffolds. (b) X-ray diffraction (XRD) patterns. (c) Scanning electron microscopy (SEM) representative images. Scale bar = 200 μm. Statistical significance: *p < 0.05.

Table 2
Pore size and porosity of engineered scaffolds.

Scaffold type	Pore size (μm)	Porosity (%)
SUM0	100.00 ± 17.16	68.33
SUM0.5	81.17 ± 7.47	47.43
SUM1	60.33 ± 12.89	42.76
SUM2	48.29 ± 18.35	29.81

enzymatically cross-linked gelatin network, the inorganic nanoclay-based interface was evaluated. Gradual incorporation of Sumecton into gelatin-based hydrogels led to up to four levels of reinforcement and four distinct approaches (SUM0, SUM0.5, SUM1, SUM2) (Fig. 1a). Initially, principal characteristics of the designed scaffolds were analyzed and, subsequently, shortlisted the foremost candidates to be further evaluated in cell and animal studies.

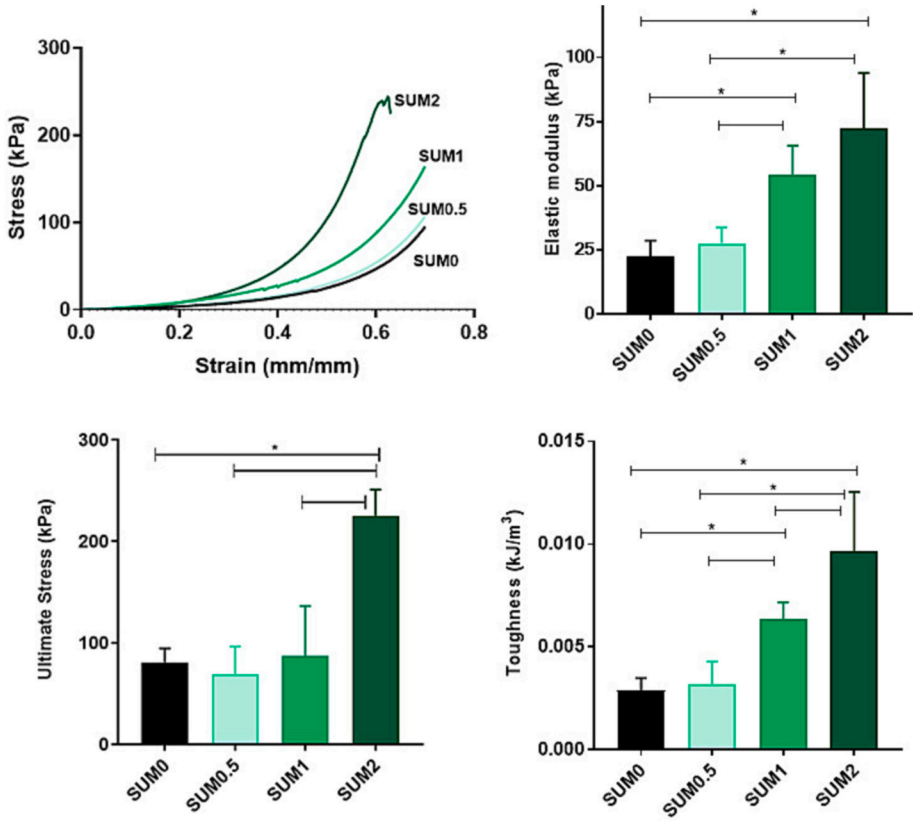

Fig. 4. Biomechanical study. Compressive stress-strain curve, elastic modulus, ultimate stress and toughness. Statistical significance: *p < 0.05.

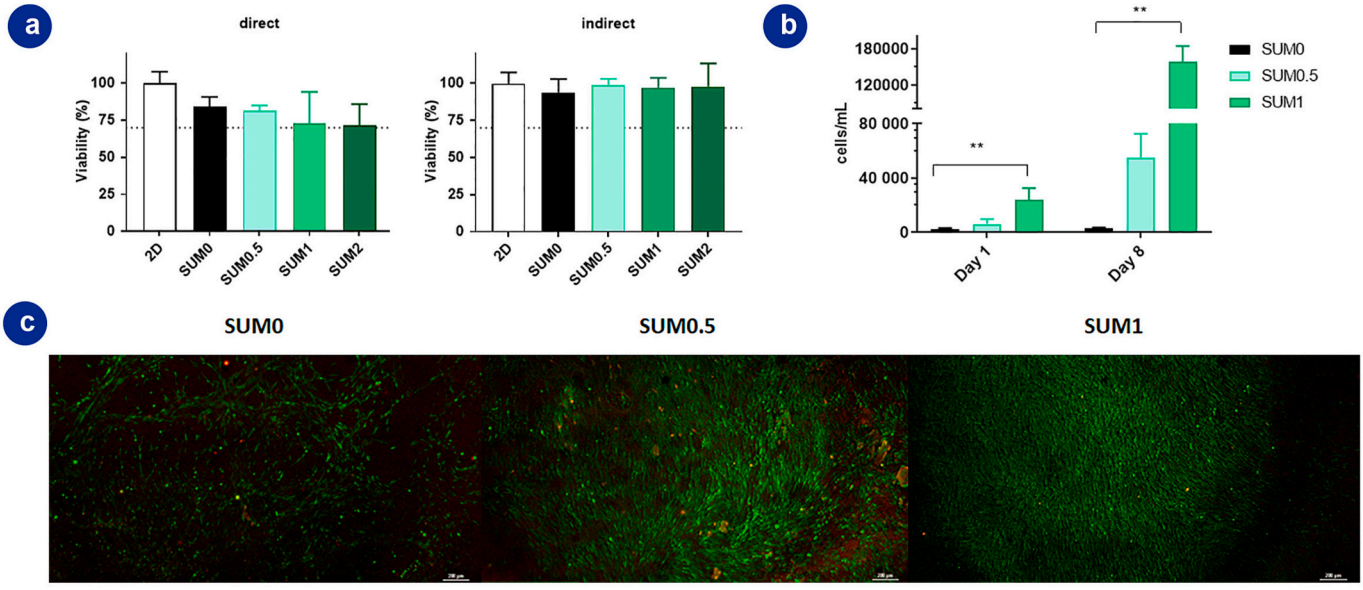

Fig. 5. Cell-scaffold interaction. (a) Biocompatibility test by direct contact and extracts. (b) Quantification of cellular viability in respective scaffolds after 8 days of culture by flow cytometry. (c) Live/Dead staining after 8 days of cell culture. Scale bar = 200 μm. Statistical significance: **p < 0.01.

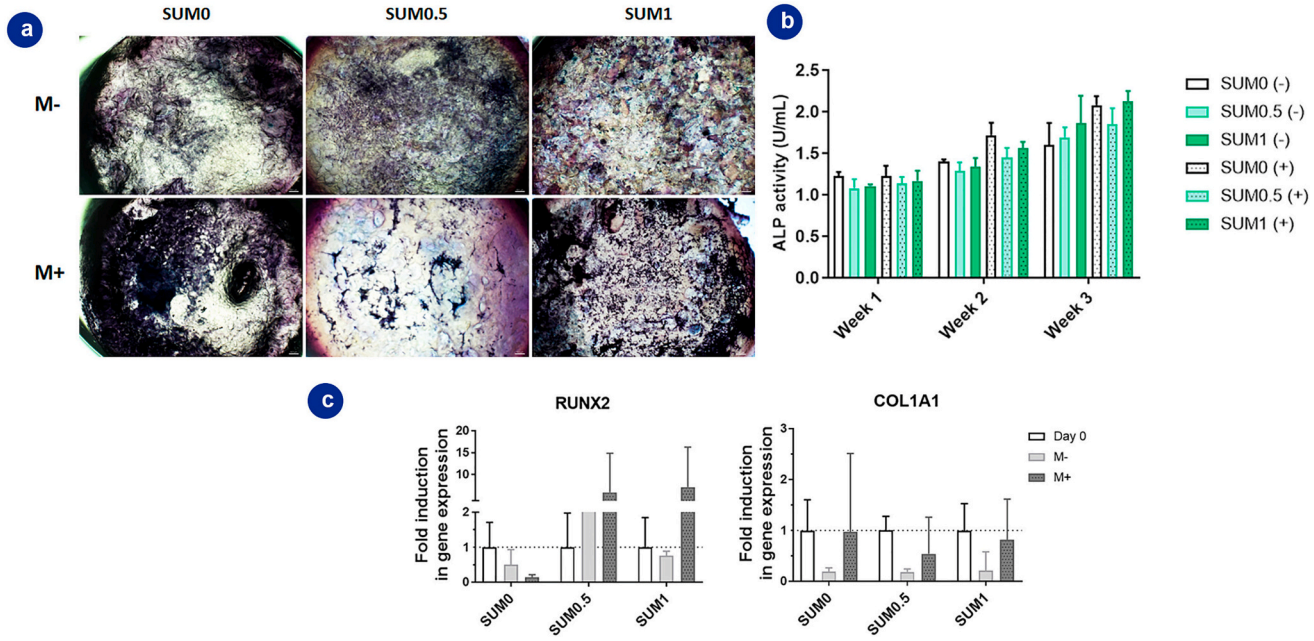

Fig. 6. Osteogenic commitment of murine bone-marrow derived mesenchymal stem cells (mBM-MSCs). (a) Alkaline phosphatase (ALP) representative staining images. Scale bar = 500 μm. (b) ALP activity secreted by mBM-MSCs after 1, 2 and 3 weeks of culture in normal media (−) and differentiation media (+). (c) Gene expression of osteogenic markers (Runx2 and Col1a1) at day 0 and 5 days post-incubation with scaffolds in normal media (M−) and differentiation media (M+).

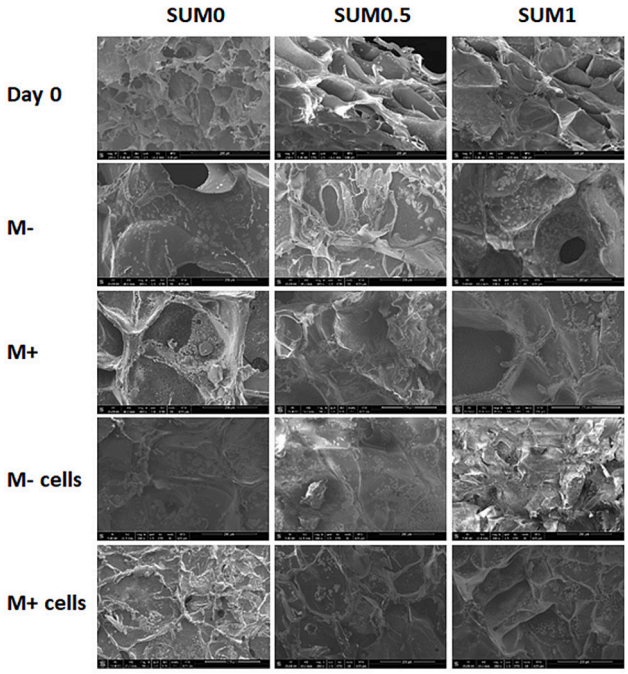

Fig. 7. SEM images of scaffolds after 5 weeks of incubation. Scaffolds at day 0 (day 0); after the incubation period in normal and differentiation media (M− and M+, respectively). Fabricated hydrogels after being in contact with cells in the determined period in normal and differentiation media (M− cells and M+ cells, respectively). Scale bar = 200 μm.

3.1. Swelling ability, degradation profile and protein adsorption

Swelling properties of freeze-dried scaffolds were determined following a previously employed formula (Eq. (1)). Wettability is essential to achieve favorable absorption of body fluids and nutrients as well as metabolites transference. Besides, swelling capability provides insight into the potential interaction between systems and surroundings, yet it needs to be closely regulated to not provoke a fast degradation [31]. Incorporation of nanoclays did not have any impact on swelling kinetics and scaffolds were totally hydrated in 2 h. Yet, not all scaffolds had the same swelling capacity. Thus, after 24 h of hydration, the swelling ratio was inversely proportional to the nanoclay concentration (Fig. 1b). Specifically, there is a statistically significant reduction of swelling ratio between control and SUM2. This data is consistent with recently described research in which swelling ratio of reinforced gelatin-based scaffolds diminished with higher nanoclay concentration [32].

A temporary construct that supports new tissue ingrowth while its degradation is synchronized with the process of regeneration remains a critical concern. Therefore, biodegradability is regarded to be one of the foremost desired attributes that a system designed for bone tissue regeneration is expected to exhibit [33]. All formulations happened to be stable within 21 days under hydrolytic environment (Fig. 1c). Those reinforced with Sumecton showed lower degradation, which confirmed the capability of nanoclays to form a solid and stable network with gelatin [34]. However, as 3D hydrogels were placed in an enzyme-rich buffer for better simulating the *in vivo* milieu, upon 4 h samples were completely degraded. Yet, the amount of protein quantified in the supernatant, due to hydrogel degradation, decreased with increasing Sumecton concentration (Fig. 2a). This phenomenon verifies the ability of nanoclays to create stiffer and more rigid scaffolds, which may undergo less degradation in an enzymatic environment [35,36].

In addition to proper micro- and nanostructure, scaffolds for bone tissue engineering must exhibit suitable protein adsorption performance. The interaction with the native surrounding medium occurs along with protein adsorption after implantation of a tissue-engineered system [37]. The latter has the potential to promote cell-scaffold interactions, which ultimately results in improved cell adhesion, viability and proliferation [37,38]. In the present work, SUM2 scaffold demonstrated a favorable and statistically significant capability to absorb proteins as compared to SUM0 (Fig. 2b), a fact that may derive from the electrostatic linkages between Sumecton and proteins [39].

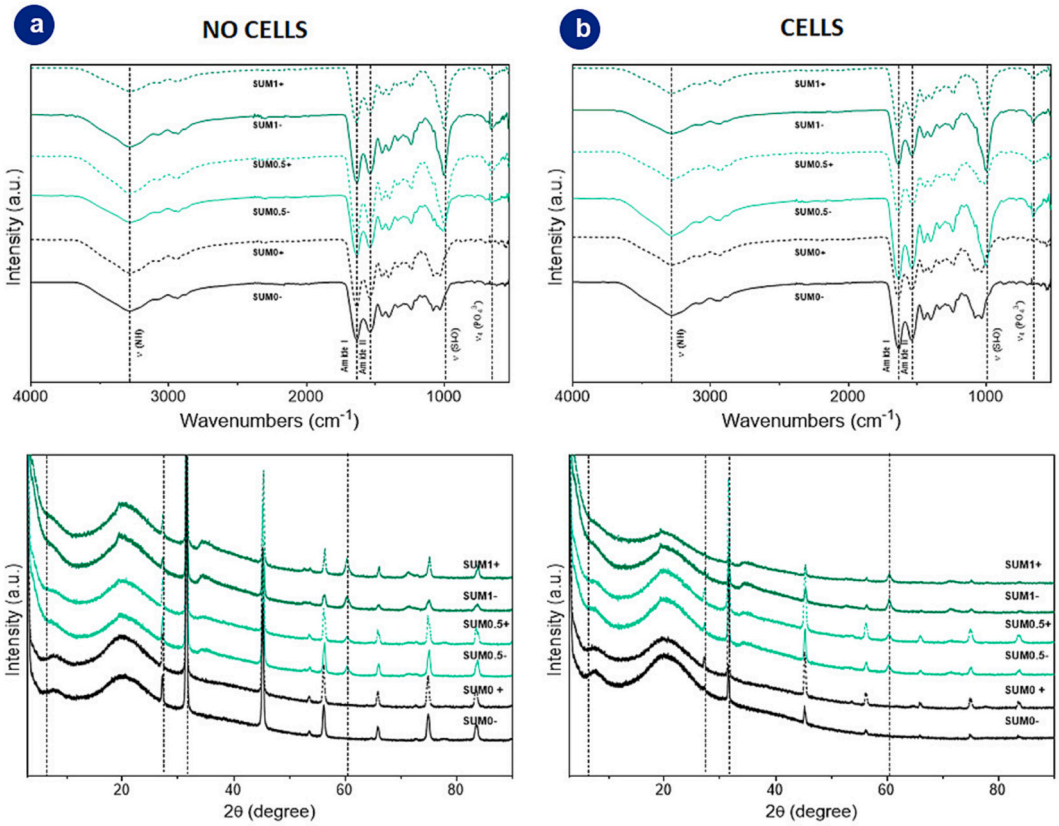

Fig. 8. Mineralization studies after 5 weeks (I). (a) FTIR and XRD patterns for the mineralization analysis of fabricated hydrogels in differentiation media (+) and normal media (−). (b) FTIR and XRD patterns for the mineralization analysis of fabricated hydrogels after cell culture in differentiation media (+) and normal media (−).

3.2. Determination of microstructure and elemental composition

Chemical interaction of gelatin network during the enzymatic crosslinking and interaction of silicate-derived materials into 3D the gelatin network were evaluated using FTIR and XRD. The existence of Sumecton was corroborated by FTIR spectra as shown in Fig. 3a. All scaffolds confirmed previously described gelatin characteristics bands in 1040 (C-O-C stretching), 1545 (Amide II) and 3306 (Amine peak) cm^{-1} [12]. In addition, silicate band (Si—O) was observed at 1025 cm^{-1} in these composite scaffolds. Reinforcement with Sumecton led to higher peak in the stretching vibration C-O-C. XRD analysis of pure Sumecton (Fig. 3b) showed peaks at 2θ value of 6.09°, 19.5°, 34.6° and 60.3°, which are consistent with previous studies [40]. After incorporation of Sumecton in to gelatin scaffolds, the higher concentrations of scaffolds shows the characteristic peaks 19.5°, 34.6° and 60.3° confirms the presence of Sumecton in the composites. However, the peak at 2θ value of 6.09° corresponded to the intermolecular interaction between 2 nanoclays that disappeared in the composites scaffolds, indicating the complete exfoliation of Sumecton in the hydrogel network.

Microstructure and pore size characterization of freeze-dried scaffolds were done using SEM in order to better understand the swelling as well as mechanical behavior of designed scaffolds. Overall, as bone matrix is an interporous tissue, high porosity (>60 %) is desirable to ensure cell-infiltration and cell-scaffold interaction. In this case, scaffolds exhibited an interconnected porosity structure, which is crucial for tissue regeneration as it is considered to influence cell interaction, migration, proliferation, and differentiation [41–43]. Specifically, 3D scaffolds with a pore size 50–100 μm have demonstrated an efficient dissemination of oxygen and diffusion of waste and nutrients between the infiltrating cells and the surroundings. Thus, osteoblast migration and proliferation are promoted, leading to bone regeneration [44,45].

As shown in Fig. 3c and detailed in Table 2, the pore size was measured in terms of diameter and all samples varied from 50 to 100 μm and porosity from 29 to 68 %, but both parameters tended to decrease as Sumecton was included into these scaffolds. This is consistent with previous research indicating that nanoclay addition may increase crosslinking density and fiber arrangement and thus reduce pore size [27,46]. Consequently, while pore diameter and porosity reduction can be proportionate to mechanical performance improvement, certain properties such as swelling capacity or cell proliferation may be compromised [41,43].

3.3. Mechanical characterization

Biomechanical properties play an important role in the field of bone tissue engineering since bone matrix is well-known for its high strength and strong toughness [47]. To ascertain that the engineered hydrogels were suitable for load-bearing tissues, as in this case bone, mechanical compression tests were performed to determine the elastic modulus, ultimate stress - the maximum stress withstood before failure - and toughness - area under the stress-strain curve - of the designed scaffolds.

When the nanomaterial was integrated into the 3D hydrogels, resulted in an increased compressive strength (toughness, elastic modulus and ultimate stress) (Fig. 4). SUM2 data indicated a statistically significant increment in the abovementioned parameters; in fact, SUM2 values were three times superior compared to SUM0, elastic modulus was ~23 kPa *vs* ~72 kPa and ultimate stress was ~225 *vs* ~80 kPa.

As in previous studies, results from this first approach were quite different from those described for bone matrix - 15–25 GPa for elastic modulus and 2–7 kJ/m^2 for toughness- [41,47]. Albeit the capacity to dissipate energy may not have been matched the osseous milieu, the elastic modulus values were between 25 and 60 kPa. The latter was in

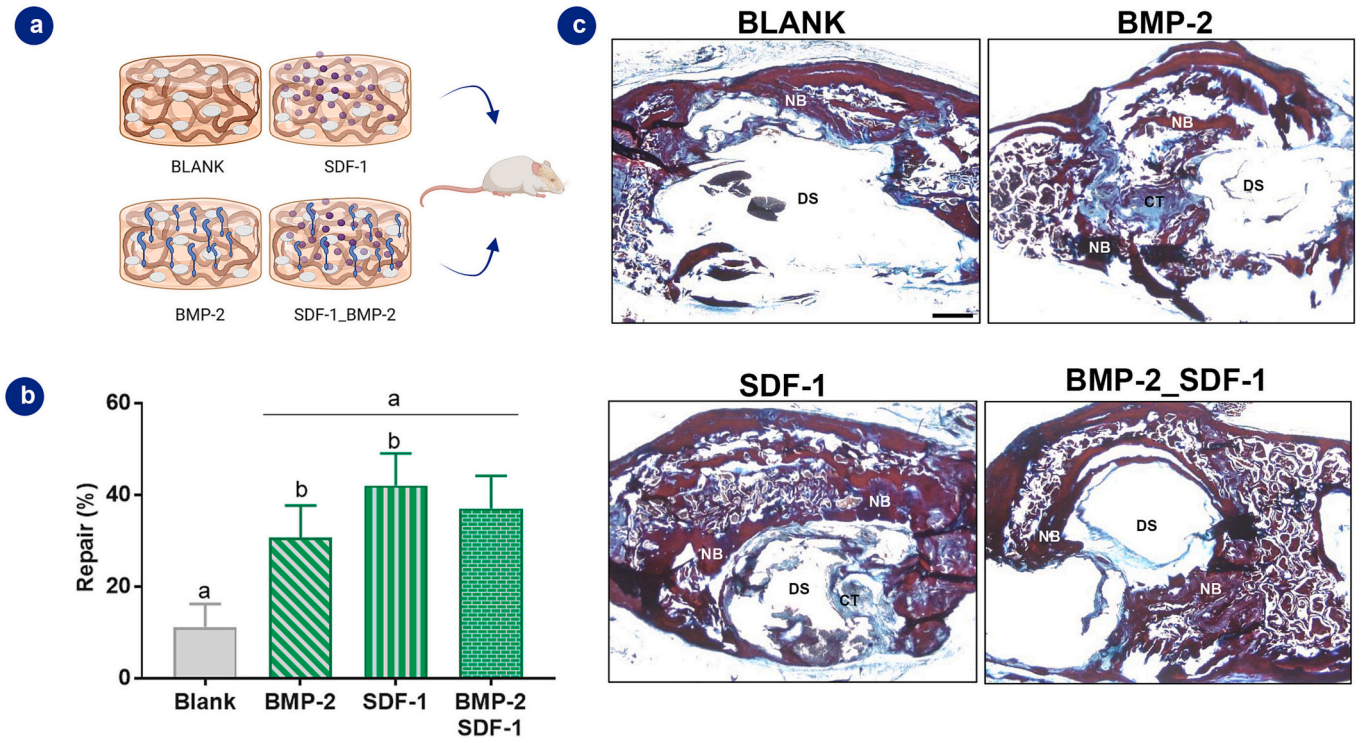

Fig. 9. Osseous repair evaluation after 8 weeks of hydrogels implantation. (a) Schematic illustration of treatment groups. (b) Histomorphometric analysis showing the percentage of repair among all experimental groups (c) Cross-sectional representative images stained with VOF of the defect site in the different experimental groups. All images show the areas of regenerated bone (NB) and bone structure. Same letters displayed in different histograms denote significant differences ($p < 0.001$) among these groups. CT: Connective tissue, DS: Defect site, NB: Newly formed bone. Scale bar = 500 μm.

accordance with previous studies that reported it to be sufficient to promote osteogenesis [48,49]. It was also worth considering the inclusion of the nanomaterials increased these values, resulting in hydrogels with stiffer properties for bone regeneration.

3.4. Biological performance

In this section, cell-scaffold interaction was studied. Albeit the results obtained in the characterization tests, SUM2 group was no longer studies, since they have shown to be not so biocompatible (described in Section 3.4.1).

3.4.1. Biocompatibility study

Cytocompatibility is among one of the main considerations when developing tissue engineering constructs [50,51]. All formulations in the present study were evaluated in accordance with ISO 10993 standard for "Biological evaluation of medical devices". The guideline defines cell viability as no <70 % compared to control. Direct and indirect tests determine non-toxicity of scaffolds and their extracts, respectively. There were no significant differences between the control and the samples and all formulations performed above 70 % of viability in both tests. Since gelatin-based hydrogels contain RGD sequences within their structures, cells were unintentionally detached prior to measuring and direct contact test values were closer to the threshold [52].

Therefore, according to ISO requirements, these systems may be contemplated non-cytotoxic for further *in vitro* studies (Fig. 5a). Nonetheless, following cell experiments were confined to 3 groups (SUM0, SUM0.5, SUM1). While all engineered structures demonstrated to be above the threshold of biocompatibility, a balance of biological and mechanical properties was taken into account and SUM2 was not further evaluated.

3.4.2. Cell viability after 8 days

To further evaluate the interaction between cells and scaffolds, mBM-MSCs viability was determined 8 days post-seeding. Cell quantification by flow cytometry evidenced the ability of all designed scaffolds to promote cell viability (Fig. 5b). All samples presented a statistically significant increase in cell population after being exposed to scaffolds for a period of 8 days. Live/Dead assay depicted a high percentage of live cells within a week of contact with scaffolds (Fig. 5c).

Within this framework, several studies have confirmed that gelatin has the capacity to promote cell proliferation, since it has RGD sequences in its polymeric structure [12,13]. The assay helped to elucidate that synthetic saponite had not have an adverse effect in cell survival, which goes in accordance with other previous studies [23,53].

3.5. Osteogenic commitment

The bone differentiation ability of mBM-MSCs seeded on the developed hydrogels involved determining ALP activity and gene expression osteogenic markers. ALP is regarded as a marker of early-stages of osteogenesis and provides an insight into the differentiation of mBM-MSCs [54]. Therefore, the activity of this enzyme was measured in terms of intracellular activity during 21 days and optical images were obtained after 21 days of post-seeding. As shown in Fig. 6a,b, there is an upward tendency in the activity over the weeks of this early marker. In fact, overall, it can be perceived that samples incubated with differentiation medium had a superior enzyme activity. The latter is confirmed with dyed samples after completion of the experiment. Optical images showed that scaffolds incubated with differentiation medium had more violet dots compared to normal medium. In the SUM1 group, the area appeared slightly more purple compared to the others.

On the other hand, in the first approach to acquire knowledge about gene commitment in the differentiation process, osteogenic (*Runx2* and *Col1a1*) genes were analyzed. As depicted in Fig. 6c, osteogenic genes

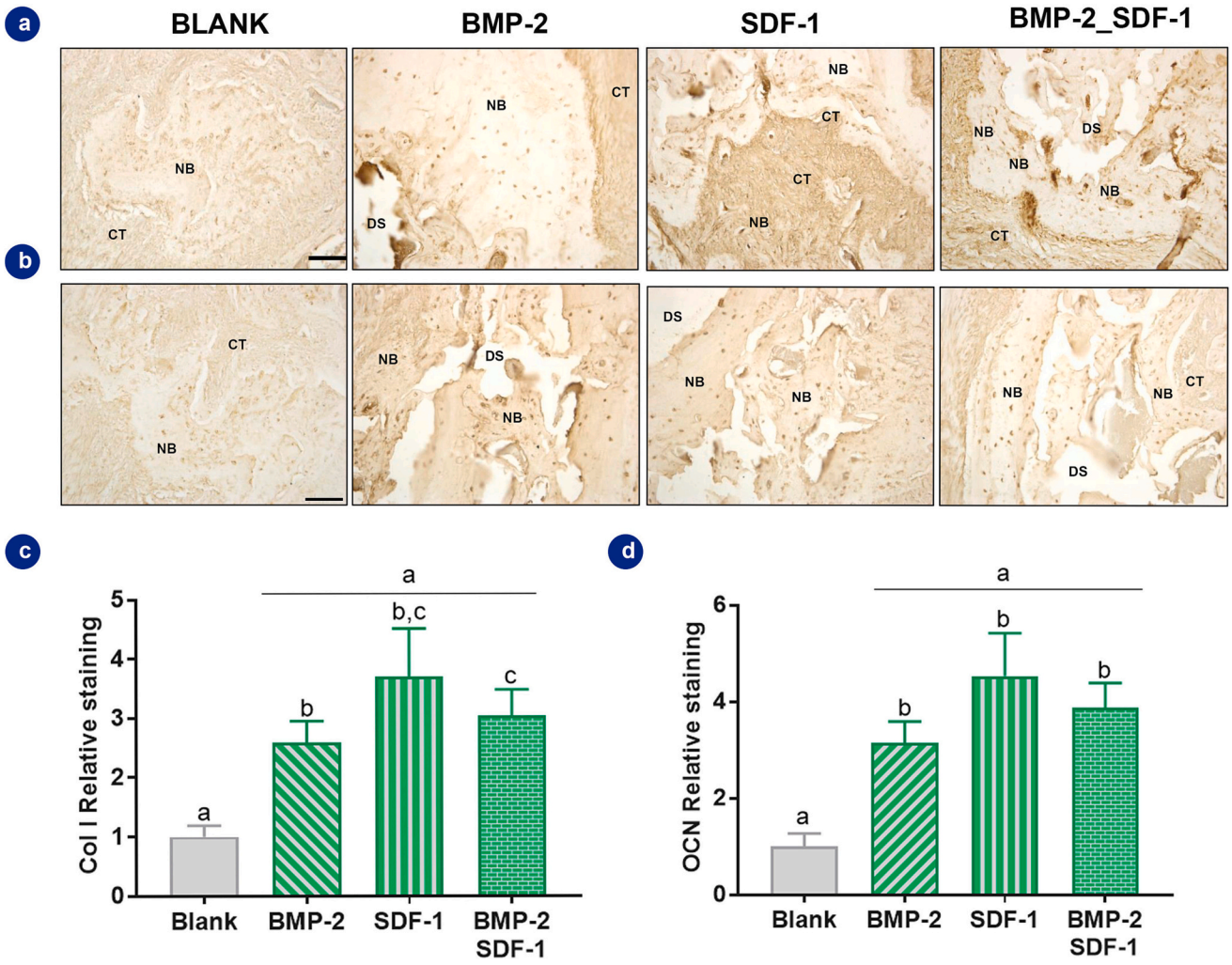

Fig. 10. Immunochemistry evaluation of newly formed bone. (a) Representative staining images of Col I in horizontal section. (b) Cross-sectional representative illustration of OCN staining. (c) Relative Col I staining is represented in arbitrary units. (d) Relative OCN staining is graphed in arbitrary units. All histograms represent the mean ± SD. Same letters on different histograms indicates significant differences ($p < 0.05$) within groups. CT: Connective tissue, NB: Newly formed bone. Scale bars = 80 μm.

were upregulated which it can be concluded that scaffold-treated cells underwent differentiation. In particular, *Runx2* expression variation was more pronounced than in *Col1a1*. This phenomenon has been described in previous studies concluding that *Runx2* expression may lead to up-regulation of *Col1a1* [55,56]. Additionally, notable differences in gene expression were found in scaffolds incubated with supplemented media in comparison to basal media. This further confirmed the ability of bone-conditioned media to enhance cell differentiation.

Overall, results are in accordance with previous studies [12,23,43]. It can be thus concluded that while gelatin itself may have osteogenic properties, bone-matrix elements (*i.e.* Ag, Mg, silicate) released from nanoclays might further enhanced them. Despite a general upregulation, scaffolds treated with differentiation medium, which was even more supplemented with osteogenic agents such as dexamethasone, showed an increased ability to differentiate towards to osteogenic lineage.

3.6. Mineralization

Upon an extended 5 weeks of incubation, mineralization process was examined chemically in terms of SEM, FTIR and XRD. SEM analysis confirmed apatite forms in all samples. In comparison to day 0, engineered scaffolds incubated in normal and differentiation media showed crystal formation both in samples after being in contact with cells and the ones with no cells (Fig. 7). Hydrogels with higher reinforcement (SUM1) and contact with cells had more mineralized structures in comparison to pristine scaffolds (SUM0).

This data was further supported with FTIR and XRD analysis. FTIR spectrum displayed hydroxyapatite presence at $\nu 4$ ($PO4^{3-}$) in all samples (Fig. 8a). However, reinforced hydrogels showed a sharper band at 1029 cm^{-1} corresponding to the Si—O of Sumecton nanocomposite and phosphate group of the hydroxyapatite. Similarly, XRD patterns confirmed hydroxyapatite-related peaks (0 0 2) and (2 1 1) in almost all samples (Fig. 8b) [12,23,27].

All these observations demonstrate on the one hand that the presence of Sumecton induces mineralization and, in turn, that the designed scaffold is biologically active.

3.7. In vivo studies

After confirming potential *in vitro* ability, SUM1 scaffolds were selected for *in vivo* assessment. This experiment was performed based on previous studies [12,23]. The latter included growth factors to promote bone regeneration. In this case, the addition of these agents was interesting mainly for two motives. On the one hand, to reaffirm the regenerative capacity of these bioactive molecules. On the other hand, to determine the potential these nanoparticles might have in the scaffold to

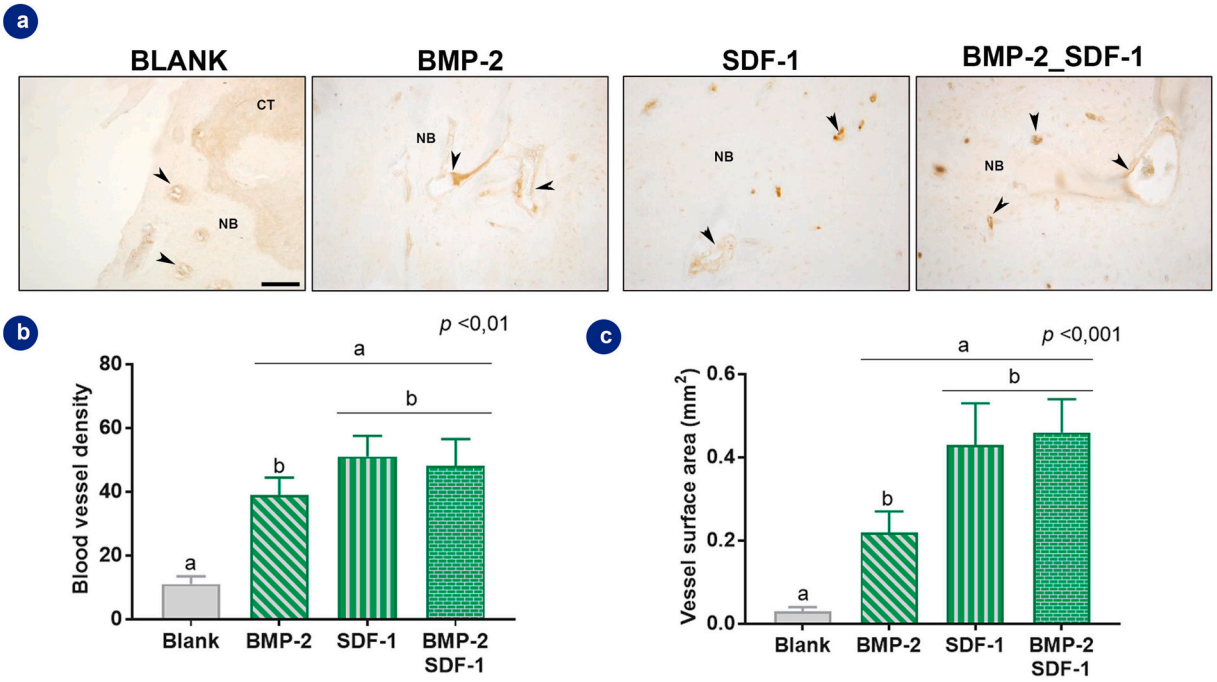

Fig. 11. Neovascularization analysis 8 weeks postimplantation of designed scaffolds. (a) Representative images in horizontal section showing CD34 immunoreactive staining, in the defect site. Immunoreaction is observed in the endothelial cells lining the lumen of blood vessels of different sizes (arrowheads). (b) Blood vessel density and (c) vessel surface area (mm^2) within the ROI among all treatment groups. Histograms represent the mean ± SD. The same letters on different histograms indicates significant differences between these groups. CT: Connective tissue. NB: Newly formed bone. Scale bar = 80 μm.

act as a drug delivery system. Since preceding research exploit BMP-2 and SDF-1, the present work will explore them separately, as well as the combination of both. Therefore, animals were classified into four treatment groups: blank (scaffolds with no growth factors), scaffolds charged either with SDF-1 or BMP-2 and a combination of SDF-1 and BMP-2 (Fig. 9a).

In regard to new bone formation, the histomorphometric analysis demonstrated a repair response rate of <20 % in the blank group, while in the growth factor-loaded scaffold groups a significant increase in repair percentages was observed with values of 30.6 % in the BMP-2 group and 42 % in the SDF-1 group, the latter showed the greatest repair response (Fig. 9b).

The histological analysis of the samples revealed few newly formed bone in blank group animals. This was mainly circumscribed to the defect edges while the rest of the defect was occupied by connective tissue (Fig. 9c). In the treated animals new bone growth was increased, both in the margins of the defect and in more extensive regions, with the central region of the defect remaining without visible signs of repair (Fig. 9c). The regenerated bone in all the experimental groups showed structural characteristics that were compatible with mature and well-mineralized bone, as evidenced by VOF trichrome staining.

Histological and histomorphometric data was also confirmed with osteogenesis-related markers analysis. Early and late osteogenesis markers- Col I and OCN, respectively, revealed a higher level of relative expression both in BMP-2 and SDF-1-treated groups compare to blank group (Fig. 10a,c). SDF-1-treated group showed the highest relative staining and it was statistically significant in contrast with BMP-2 and BMP-2_SDF-1 group (Fig. 10b,d).

Lastly, since forming new blood-vessels plays a key role in the bone regeneration process, it was analyzed with the vascular indicator anti-CD34. All groups showed a relatively even distribution of neo-vascularization in the regenerated tissue. Analysis on regenerated bone revealed the existence of superior density and vascular surface area among treated animals when compared to the blank group, especially in the SDF-1-treated ones (Fig. 11).

Regarding the ability of the designed scaffolds, the conclusion to be drawn from this study is that cell-free scaffolds have osteogenic as well as osteoinductive properties. Yet, as previously reported, it is essential to supplement scaffolds with bioactive agents to achieve an optimal osseoregeneration [12,23,57]. In particular, SDF-1 in comparison with BMP-2 has shown to be more effective which may be due to its mechanism of action. While SDF-1 is a chemokine that plays a key role in stem cells recruitment in the damaged area, BMP-2 induces stem cell differentiation [58,59]. BMP-2 likewise has repair capacity, but it is possible that 8 weeks may not be sufficient to notice these improvements in the healing process. There are also many other factors that should be considered in the future such as dose or agent properties.

Ideally, it was expected to obtain a synergistic effect with BMP-2_SDF-1 concomitant treatment group, but all gathered data showed higher bone growth in SDF-1 experimental group. Certainly, it has been previously described that a co-treatment with both bioactive peptides is not necessarily associated with improved outcomes [60]. Nonetheless, another study tailored the release of these bioactive agents by considering the role of each one. SDF-1 was released from an early stage in order to attract mesenchymal stem cells and BMP-2 had a controlled delivery since it plays a role in the induction of osteodifferentiation. Thus, sequential delivery showed higher bone regeneration ability in rat animal models [61]. This phenomenon should be taken into consideration in forthcoming studies.

4. Conclusion

In the current study, biologically inspired and mechanically reinforced three dimensional scaffolds were designed. For that, saponite-derived clay was combined within a gelatin network. The constructs demonstrated favorable *in vitro* performance in terms of pore size, compressive properties and biocompatibility for healing bone defects. Similarly, the osteoconductive nanoclay-reinforced gelatin composites loaded with biologically active factors promoted bone regeneration in animal model. Overall, results showed that engineered nanoreinforced

polymeric 3D systems may be effective to serve as biomimetic molecules-delivery platform for bone regeneration, preventing high doses and cell-laden systems. Thereby, possible negative effects could be mitigated and would be more cost-effective. Albeit it has proven to be suitable for bone tissue engineering, further studies are needed, as the ideal system should exclude the addition of biological agents.

CRediT authorship contribution statement

Izeia Lukin: Conceptualization, Investigation, Formal analysis, Writing – original draft, Visualization. **Itsasne Erezuma:** Investigation, Writing – original draft, Writing – review & editing. **Patricia Garcia-Garcia:** Investigation. **Ricardo Reyes:** Investigation. **Carmen Evora:** Investigation. **Firoz Babu Kadumudi:** Investigation. **Alireza Dolatshahi-Pirouz:** Conceptualization, Supervision, Project administration. **Gorka Orive:** Conceptualization, Supervision, Project administration.

Declaration of competing interest

The authors declare that they have no known competing financial interests or personal relationships that could have appeared to influence the work reported in this paper.

Acknowledgements

Graphical abstract was created using BioRender.com. This work was assisted by the Spanish Ministry of Science and Innovation (PID2022-139746OB-I00/AEI/10.13039/501100011033) and technical support from the ICTS NANBIOSIS (Drug Formulation Unit, U10) at the University of the Basque Country. We are also gratefully appreciative of the support from the Basque Country Government (Grupos Consolidados, No ref: IT907-16). I. Lukin and I. Erezuma acknowledge the Basque Government for the PhD grants (PRE_ 2022_2_0041 & PRE_2021_2_0023). A.D.-P. would like to thank to the Danish Council for Independent Research (Technology and Production Sciences, 8105–00003B), and the VIDI research programme (Project number R0004387), which is (partly) financed by The Netherlands Organisation for Scientific Research (NWO). This work has also received funding from the European Union's Horizon 2020 research and innovation programme under grant agreement No 951747.

References

[1] A. Wu, C. Bisignano, S.L. James, G.G. Abady, A. Abedi, E. Abu-Gharbieh, et al., Global, regional, and national burden of bone fractures in 204 countries and territories, 1990–2019: a systematic analysis from the Global Burden of Disease Study 2019, Lancet Healthy Longev. 2 (2021) e580–e592.
[2] F. Borgström, L. Karlsson, G. Ortsäter, N. Norton, P. Halbout, C. Cooper, et al., Fragility fractures in Europe: burden, management and opportunities, Arch. Osteoporos. 15 (2020) 59.
[3] E. Lavik, R. Langer, Tissue engineering: current state and perspectives, Appl. Microbiol. Biotechnol. 65 (2004) 1–8.
[4] C.P. Pennisi, C. Sevcencu, A. Dolatshahi-Pirouz, M. Foss, J.L. Hansen, A.N. Larsen, et al., Responses of fibroblasts and glial cells to nanostructured platinum surfaces, Nanotechnology. 20 (2009) 385103–385109.
[5] M.N. Collins, G. Ren, K. Young, S. Pina, R.L. Reis, J.M. Oliveira, Scaffold fabrication technologies and structure/function properties in bone tissue engineering, Adv. Funct. Mater. 31 (2021), 2010609 (n/a).
[6] T. Jensen, T. Jakobsen, J. Baas, J.V. Nygaard, A. Dolatshahi-Pirouz, M. B. Hovgaard, et al., Hydroxyapatite nanoparticles in poly-D,L-lactic acid coatings on porous titanium implants conducts bone formation, J. Biomed. Mater. Res. A 95A (2010) 665–672.
[7] T. Jensen, A. Dolatshahi-Pirouz, M. Foss, J. Baas, J. Lovmand, M. Duch, et al., Interaction of human mesenchymal stem cells with osteopontin coated hydroxyapatite surfaces, Colloids Surf. B: Biointerfaces 75 (2010) 186–193.
[8] B. Salahuddin, S. Wang, D. Sangian, S. Aziz, Q. Gu, Hybrid gelatin hydrogels in nanomedicine applications, ACS Appl. Bio Mater. 4 (2021) 2886–2906.
[9] I. Lukin, I. Erezuma, L. Maeso, J. Zarate, M.F. Desimone, T.H. Al-Tel, et al., Progress in gelatin as biomaterial for tissue engineering, Pharmaceutics. 14 (2022) 1177.
[10] K. Zhang, S. Wang, C. Zhou, L. Cheng, X. Gao, X. Xie, et al., Advanced smart biomaterials and constructs for hard tissue engineering and regeneration, Bone Res. 6 (2018) (31-15).
[11] J. Wu, H. Shin, J. Lee, S. Kim, H. Lee, Preparation of external stimulus-free gelatin–catechol hydrogels with injectability and tunable temperature responsiveness, ACS Appl. Mater. Interfaces 14 (2022) 236–244.
[12] M.C. Echave, I. Erezuma, N. Golafshan, M. Castilho, F.B. Kadumudi, C. Pimenta-Lopes, et al., Bioinspired gelatin/bioceramic composites loaded with bone morphogenetic protein-2 (BMP-2) promote osteoporotic bone repair, Mater. Sci. Eng. C 112539 (2021).
[13] M.C. Echave, C. Pimenta-Lopes, J.L. Pedraz, M. Mehrali, A. Dolatshahi-Pirouz, F. Ventura, et al., Enzymatic crosslinked gelatin 3D scaffolds for bone tissue engineering, Int. J. Pharm. 562 (2019) 151–161.
[14] S. Ranganathan, K. Balagangadharan, N. Selvamurugan, Chitosan and gelatin-based electrospun fibers for bone tissue engineering, Int. J. Biol. Macromol. 133 (2019) 354–364.
[15] S. Sharifi, M.M. Islam, H. Sharifi, R. Islam, D. Koza, F. Reyes-Ortega, et al., Tuning gelatin-based hydrogel towards bioadhesive ocular tissue engineering applications, Bioact. Mater. 6 (2021) 3947–3961.
[16] A. Serafin, C. Murphy, M.C. Rubio, M.N. Collins, Printable alginate/gelatin hydrogel reinforced with carbon nanofibers as electrically conductive scaffolds for tissue engineering, Mater. Sci. Eng. C 122 (2021), 111927.
[17] Y.P. Singh, A. Bandyopadhyay, B.B. Mandal, 3D bioprinting using cross-linker-free silk–gelatin bioink for cartilage tissue engineering, ACS Appl. Mater. Interfaces 11 (2019) 33684–33696.
[18] M.C. Echave, L. Saenz del Burgo, J.L. Pedraz, G. Orive, Gelatin as biomaterial for tissue engineering, Curr. Pharm. Des. 23 (2017) 3567–3584.
[19] D. Lopes, C. Martins-Cruz, M.B. Oliveira, J.F. Mano, Bone physiology as inspiration for tissue regenerative therapies, Biomaterials. 185 (2018) 240–275.
[20] Z. Yuan, X. Yuan, Y. Zhao, Q. Cai, Y. Wang, R. Luo, et al., Injectable GelMA cryogel microspheres for modularized cell delivery and potential vascularized bone regeneration, Small. 17 (2021), e2006596 (n/a).
[21] K. Yue, G. Trujillo-de Santiago, M.M. Alvarez, A. Tamayol, N. Annabi, A. Khademhosseini, Synthesis, properties, and biomedical applications of gelatin methacryloyl (GelMA) hydrogels, Biomaterials. 73 (2015) 254–271.
[22] X. Zhou, J. Sun, K. Wo, H. Wei, H. Lei, J. Zhang, et al., nHA-loaded gelatin/alginate hydrogel with combined physical and bioactive features for maxillofacial bone repair, Carbohydr. Polym. 298 (2022), 120127.
[23] I. Erezuma, I. Lukin, C. Pimenta-Lopes, F. Ventura, P. Garcia-Garcia, R. Reyes, et al., Nanoclay-reinforced HA/alginate scaffolds as cell carriers and SDF-1 delivery-platforms for bone tissue engineering, Int. J. Pharm. 623 (2022), 121895.
[24] I. Erezuma, T. Eufrasio-da-Silva, N. Golafshan, K. Deo, Y.K. Mishra, M. Castilho, et al., Nanoclay reinforced biomaterials for mending musculoskeletal tissue disorders, Adv. Healthc. Mater. 10 (2021), 2100217 (n/a).
[25] M. Mehrali, A. Thakur, C.P. Pennisi, S. Talebian, A. Arpanaei, M. Nikkhah, et al., Nanoreinforced hydrogels for tissue engineering: biomaterials that are compatible with load-bearing and electroactive tissues, Adv. Mater. 29 (2017), 1603612 (n/a).
[26] X. Zheng, X. Zhang, Y. Wang, Y. Liu, Y. Pan, Y. Li, et al., Hypoxia-mimicking 3D bioglass-nanoclay scaffolds promote endogenous bone regeneration, Bioact. Mater. 6 (2021) 3485–3495.
[27] M. Hasany, A. Thakur, N. Taebnia, F.B. Kadumudi, M. Shahbazi, M.K. Pierchala, et al., Combinatorial screening of nanoclay-reinforced hydrogels: a glimpse of the "holy grail" in orthopedic stem cell therapy? ACS Appl. Mater. Interfaces 10 (2018) 34924–34941.
[28] M. Rodríguez-Évora, A. Delgado, R. Reyes, A. Hernández-Daranas, I. Soriano, J. San Román, et al., Osteogenic effect of local, long versus short term BMP-2 delivery from a novel SPU–PLGA–βTCP concentric system in a critical size defect in rats, Eur. J. Pharm. Sci. 49 (2013) 873–884.
[29] A. Hernández, R. Reyes, E. Sánchez, M. Rodríguez-Évora, A. Delgado, C. Évora, In vivo osteogenic response to different ratios of BMP-2 and VEGF released from a biodegradable porous system, J. Biomed. Mater. Res. A 100A (2012) 2382–2391.
[30] E. Martínez-Sanz, D.A. Ossipov, J. Hilborn, S. Larsson, K.B. Jonsson, O.P. Varghese, Bone reservoir: injectable hyaluronic acid hydrogel for minimal invasive bone augmentation, J. Control. Release 152 (2011) 232–240.
[31] L. Gu, T. Li, X. Song, X. Yang, S. Li, L. Chen, et al., Preparation and characterization of methacrylated gelatin/bacterial cellulose composite hydrogels for cartilage tissue engineering, Regen. Biomater. 7 (2020) 195–202.
[32] L. Tao, L. Zhonglong, X. Ming, Y. Zezheng, L. Zhiyuan, Z. Xiaojun, et al., In vitro and in vivo studies of a gelatin/carboxymethyl chitosan/LAPONITE® composite scaffold for bone tissue engineering, RSC Adv. 7 (2017) 541–5411.
[33] G. Chen, W. Tang, X. Wang, X. Zhao, C. Chen, Z. Zhu, Applications of hydrogels with special physical properties in biomedicine, Polymers. 11 (2019) 1420.
[34] C. Sharma, A.K. Dinda, P.D. Potdar, C. Chou, N.C. Mishra, Fabrication and characterization of novel nano-biocomposite scaffold of chitosan–gelatin–alginate–hydroxyapatite for bone tissue engineering, Mater. Sci. Eng. C 64 (2016) 416–427.
[35] C. Tipa, M. Cidade, J. Borges, L. Costa, J. Silva, P. Soares, Clay-based nanocomposite hydrogels for biomedical applications: a review, Nanomaterials 12 (2022) 3308.
[36] C. Wu, A.K. Gaharwar, P.J. Schexnailder, G. Schmidt, Development of biomedical polymer-silicate nanocomposites: a materials science perspective, Materials. 3 (2010) 2986–3005.
[37] H. Chang, Cell Responses to Surface and Architecture of Tissue Engineering Scaffolds, IntechOpen, 2011.
[38] R. Bilginer, D. Ozkendir-Inanc, U.H. Yildiz, A. Arslan-Yildiz, Biocomposite scaffolds for 3D cell culture: propolis enriched polyvinyl alcohol nanofibers favoring cell adhesion, J. Appl. Polym. Sci. 138 (2021), 50287 (n/a).

[39] A.K. Gaharwar, L.M. Cross, C.W. Peak, K. Gold, J.K. Carrow, A. Brokesh, et al., 2D nanoclay for biomedical applications: regenerative medicine, therapeutic delivery, and additive manufacturing, Adv. Mater. 31 (2019), e1900332 (n/a).
[40] K. S, R. Rama Pawar, B.D. Kevadiya, H.C. Bajaj, Synthesis of saponite based nanocomposites to improve the controlled oral drug release of model drug quinine hydrochloride dihydrate, Pharmaceuticals. 12 (2019) 105.
[41] B. Safari, M. Aghazadeh, L. Roshangar, A. Aghanejad, S. Davaran, A bioactive porous scaffold containing collagen/phosphorous-modified polycaprolactone for osteogenesis of adipose-derived mesenchymal stem cells, Eur. Polym. J. 171 (2022), 111220.
[42] B. Safari, A. Aghanejad, J. Kadkhoda, M. Aghazade, L. Roshangar, S. Davaran, Biofunctional phosphorylated magnetic scaffold for bone tissue engineering, Colloids Surf. B: Biointerfaces 211 (2022), 112284.
[43] B. Safari, M. Aghazadeh, A. Aghanejad, Osteogenic differentiation of human adipose-derived mesenchymal stem cells in a bisphosphonate-functionalized polycaprolactone/gelatin scaffold, Int. J. Biol. Macromol. 241 (2023), 124573.
[44] N. Annabi, J.W. Nichol, X. Zhong, C. Ji, S. Koshy, A. Khademhosseini, et al., Controlling the porosity and microarchitecture of hydrogels for tissue engineering, Tissue Eng. B Rev. 16 (2010) 371–383.
[45] I. Bružauskaitė, D. Bironaitė, E. Bagdonas, E. Bernotienė, Scaffolds and cells for tissue regeneration: different scaffold pore sizes—different cell effects, Cytotechnology. 68 (2016) 355–369.
[46] N. Khatoon, M.Q. Chu, C.H. Zhou, Nanoclay-based drug delivery systems and their therapeutic potentials, J. Mater. Chem. B Mater. Biol. Med. 8 (2020) 7335–7351.
[47] C. Ma, T. Du, X. Niu, Y. Fan, Biomechanics and mechanobiology of the bone matrix, Bone Res. 10 (2022) 59.
[48] J.H. Wen, L.G. Vincent, A. Fuhrmann, Y.S. Choi, K.C. Hribar, H. Taylor-Weiner, et al., Interplay of matrix stiffness and protein tethering in stem cell differentiation, Nat. Mater. 13 (2014) 979–987.
[49] S. Han, J. Kim, G. Lee, D. Kim, Mechanical properties of materials for stem cell differentiation, Adv. Biosyst. 4 (2020), e2000247 (n/a).
[50] S. Naahidi, M. Jafari, M. Logan, Y. Wang, Y. Yuan, H. Bae, et al., Biocompatibility of hydrogel-based scaffolds for tissue engineering applications, Biotechnol. Adv. 35 (2017) 530–544.
[51] A. Chyzy, M.E. Plonska-Brzezinska, Hydrogel properties and their impact on regenerative medicine and tissue engineering, Molecules. 25 (2020) 5795.
[52] J. Li, Y. Zhang, X. Zhou, S. Wang, R. Hao, J. Han, et al., Enzymatically functionalized RGD-gelatin scaffolds that recruit host mesenchymal stem cells in vivo and promote bone regeneration, J. Colloid Interface Sci. 612 (2022) 377–391.
[53] M. Ågren, Clay minerals for tissue regeneration, repair, and engineering, in: Wound Healing Biomaterials Vol. 2, Elsevier Science & Technology, United Kingdom, 2016.
[54] S. Vimalraj, Alkaline phosphatase: structure, expression and its function in bone mineralization, Gene. 754 (2020), 144855.
[55] M.J. Ortuño, A.R.G. Susperregui, N. Artigas, J.L. Rosa, F. Ventura, Osterix induces Col1a1 gene expression through binding to Sp1 sites in the bone enhancer and proximal promoter regions, Bone. 52 (2012) 548–556.
[56] T. Komori, Regulation of proliferation, differentiation and functions of osteoblasts by Runx2, Int. J. Mol. Sci. 20 (2019) 1694.
[57] Y. Chang, C. Hsieh, C. Yeh, F. Lin, The development of gelatin/hyaluronate copolymer mixed with calcium sulfate, hydroxyapatite, and stromal-cell-derived factor-1 for bone regeneration enhancement, Polymers. 11 (2019) 1454.
[58] B. Xia, Y. Deng, Y. Lv, G. Chen, Stem cell recruitment based on scaffold features for bone tissue engineering, Biomater. 9 (2021) (1189-123).
[59] Z. Liang, Y. Luo, Y. Lv, Mesenchymal stem cell-derived microvesicles mediate BMP2 gene delivery and enhance bone regeneration, J. Mater. Chem. B 8 (2020) 6378–6389.
[60] C. Lee, M.U. Jin, H. Jung, J. Lee, T. Kwon, Effect of dual treatment with SDF-1 and BMP-2 on ectopic and orthotopic bone formation, PLoS ONE 10 (2015), e0120051.
[61] X. Shen, Y. Zhang, Y. Gu, Y. Xu, Y. Liu, B. Li, et al., Sequential and sustained release of SDF-1 and BMP-2 from silk fibroin-nanohydroxyapatite scaffold for the enhancement of bone regeneration, Biomaterials. 106 (2016) 205–216.